Applied Catalysis B: Environmental 312 (2022) 121384

Contents lists available at ScienceDirect

Applied Catalysis B: Environmental

journal homepage: www.elsevier.com/locate/apcatb

Viability of $Au/La_2O_3/HAP$ catalysts for the CO preferential oxidation reaction under reformate gas conditions

Zouhair Boukha *, Juan R. González-Velasco, Miguel A. Gutiérrez-Ortiz

Chemical Technologies for Environmental Sustainability Group, Department of Chemical Engineering, Faculty of Science and Technology, University of the Basque Country UPV/EHU, P.O. Box 644, E-48080 Bilbao, Spain

ARTICLE INFO

Keywords:
Gold catalyst
Hydroxyapatite
Lanthana
Preferential oxidation of CO
Realistic conditions

ABSTRACT

The viability of gold supported on lanthanum-modified HAP catalysts is investigated for CO preferential oxidation (PROX) in H_2-rich stream. All samples comprise small nanoparticles (NPs) of Au (< 4 nm). Addition of La enhances the chemisorption of CO, whereas it lowers that of H_2 and H_2O. Moreover, lanthanum improves the reducibility of the catalysts and the mobility of oxygen. FTIR studies show that under CO oxidation conditions Au exists in two distinct forms on La-promoted samples, namely $Au^{\sigma+}$ and Au^{+} species. The catalytic tests under different PROX conditions show an improvement of the performance with lanthanum addition. The observed improvement is linked to suitable chemical properties, whereas efficiency dependence on Au NP sizes is rather secondary. At 80 °C, La-rich catalysts completely eliminate CO and prove to be selective (66%) under realistic PROX conditions (in the presence of H_2O and CO_2). Moreover, they are exceptionally stable during an extended period (240 h).

1. Introduction

The development of efficient and clean energy technologies is currently one of the most important challenges facing scientific research. In this sense, strategies based on the use of hydrogen fuel, for energy production, are very attractive to reduce carbon emission levels. Hydrogen is mainly produced through reforming processes using natural gas and, at lesser extent, renewable resources [1–6]. Typically, after a first purification stage, using water-gas shift reaction (WGSR), the resulting reformate comprises about 1% CO. However, this concentration is known to have a detrimental effect on the performance of the commonly used electrochemical devices, such as proton-exchange-membrane fuel cells (PEMFCs). For this reason, there is a renewed interest in the catalytic processes allowing the production of high-purity hydrogen presenting low concentrations of CO (< 50 ppm). Among them, the preferential oxidation (PROX) of CO is considered one of the most efficient and cost-effective solutions.

Therefore, the development of active and selective catalysts is essential for the PROX process. In the PEMFC applications, the efficient catalysts must be able to deplete CO to near-zero levels, at relatively low temperatures (80–120 °C), and the oxidation of H_2 should be minimized as much as possible [1–6]. Moreover, they should be highly resistant to deactivation under reformate streams containing high concentrations of H_2O and CO_2. According to previous reports, supported gold catalysts are promising for these demanding requirements [1–5]. Due to the critical role that plays the nature of the support, current research is mainly focused on the examination of its influence on the activity and selectivity of Au active phases. In this sense, Au catalysts have been deposited on different materials such as Fe_2O_3, TiO_2, Al_2O_3, CeO_2, HAP, ZrO_2 and ZSM-5 with the aim of finding suitable interactions metal-support that positively affect the size and the electronic properties of the Au particles [1–6]. Nevertheless, there is no consensus concerning the intrinsic Au active sites involved for an efficient CO elimination [1, 4]. Though it is widely accepted that it is essential to achieve a high dispersion and a complete reduction of gold during its activation pre-treatment, the impact of the presence of oxygen on its oxidation state, when the catalyst is working, is still not clear.

On the other hand, the use of hydroxyapatite (HAP) materials as catalyst supports has attracted great interest over the last years. Indeed, HAP-based catalysts have proved to be highly performant in a variety of catalytic processes [1,7–13]. This was explained by the suitable physicochemical properties of HAP, making it a good alternative to traditional supports. In addition, the possibility of tunning its surface properties by varying the Ca/P atomic ratio or by ionic exchanges, seems

* Corresponding author.
E-mail address: zouhair.boukha@ehu.eus (Z. Boukha).

https://doi.org/10.1016/j.apcatb.2022.121384
Received 26 January 2022; Received in revised form 3 April 2022; Accepted 5 April 2022
Available online 9 April 2022

Table 1
Composition, textural properties and TEM data for the Au/La(x)/HAP samples.

Sample	ICP-AES			BET			TEM	
	Ca/P[a]	Au, wt%	La, wt%	S_{BET}, $m^2\ g^{-1}$	V_p[b], $cm^3\ g^{-1}$	d_p[c], nm	d_{Au}[d], nm	D_{Au}[e], %
Au/HAP	1.65	1.09	0	56	0.31	20	2.8 (± 0.6)	41.7
Au/La(0.9)/HAP	1.66	1.11	0.9	48	0.31	25	2.2 (± 0.6)	50.8
Au/La(3.4)/HAP	1.63	1.10	3.4	51	0.33	26	3.6 (± 1.8)	34.0
Au/La(6.6)/HAP	1.66	1.12	6.6	43	0.29	29	1.9 (± 0.5)	57.2

[a] Ca/P atomic ratio as determined by ICP-AES.
[b] Pore volume, as determined by application of BJH method.
[c] Mean pore diameter, as determined by application of BJH method.
[d] Average Au particle size and
[e] Au dispersion, estimated by TEM.

to be very attractive, allowing the improvement of the catalytic performance. We recently reported the extraordinary performance of fluorine-substituted HAP supported gold in the PROX reaction [1]. The modification of the HAP support with fluorine resulted in a significant improvement of the activity of the Au NPs. The optimized catalyst, presenting a F-substitution degree close to 29%, proved to be efficient for the total elimination of CO at 80 °C. Likewise, it was selective and very resistant to deactivation in the presence of H_2O (15%) and CO_2 (20%). The observed improvement was explained by an increase in the proton conductivity of the support owing to the incorporation of F^- into the one-dimensional OH^- chain of the HAP lattice. This parameter was found to be extremely important allowing the effective participation of water molecules in the CO oxidation mechanism. According to Saavedra et al. [3], proton transfer at the metal-support interface facilitates the activation of O_2 to form Au-OOH intermediates, which in turn react with adsorbed CO to form Au-COOH species.

However, despite these promising results, there is still a large room of improvement of the process selectivity. Since a slight increase of selectivity can bring substantial economic returns, search for new catalytic formulations capable of maximizing the selectivity is essential. In the present work we investigate the promotional effect of lanthanum addition on the catalytic properties of the Au/HAP system in the PROX reaction. The choice of lanthanum as a promoter was made considering its capacity to generate a good ionic conductivity [7]. Furthermore, its positive effect on the PROX activity of supported gold catalysts was already described in previous reports [14–16]. The improved catalytic properties of the La-promoted samples were linked to the occurrence of suitable electronic properties of Au NPs which favor CO oxidation and minimize the competing H_2 activation. For instance, Lakshmanan et al. [14] observed that gold supported on La-modified alumina catalyst exhibited the best performance compared with those modified with Ce and Mg, respectively. The active species of the former were identified as Au NPs with a lower oxidation-state.

2. Experimental

2.1. Preparation of the catalysts

The HAP support (Ca/P = 1.69) was synthesized by co-precipitation using two aqueous solutions containing $Ca(NO_3)_2.4\ H_2O$ (1 mol L^{-1}) and $(NH_4)_2HPO_4$ (0.6 mol L^{-1}) salts, at 80 °C. The pH of the suspension was adjusted to about 10 using ammonia solution. After stirring for 16 h, the recovered solid was washed with distilled water, until reaching pH 7, and then dried at 120 °C for 12 h. The resulting HAP sample was finally heat treated in air at 500 °C for 4 h.

Au/La(x)/HAP catalysts, where "x" represents the actual loading of La (wt%), as determined by inductively coupled plasma atomic emission spectroscopy (ICP-AES), were prepared by modification of the HAP support with La and Au precursors, subsequently. First, four La doped HAP samples were prepared by impregnation, using solutions with three different amounts of the $La(NO_3)_3.6\ H_2O$ salt. The resulting samples were dried at 120 °C for 12 h, and then calcined for 4 h at 500 °C. The Au/La(x)/HAP catalysts were prepared by deposition-precipitation method with urea (DPU). The HAP and La-modified HAP samples (7 g) were suspended in an aqueous solution (210 mL) containing 2.54 $mmol_{Au}\ L^{-1}$ (using $HAuCl_4$ precursor (Aldrich)). After addition of urea (5.3 g), the suspension was stirred for 20 h at 80 °C. Finally, the recovered solids were washed and then dried at 100 °C for 12 h.

2.2. Characterization techniques

Detailed procedures for the surface area measurement by Brunauer-Emmett-Teller (BET) method, transmission electron microscopy (TEM), high-angle annular dark field (HAADF), scanning transmission electron microscopy (STEM), X-ray diffraction (XRD), X-ray photoelectron spectroscopy (XPS), oxygen storage capacity complete (OSCC), oxygen storage capacity (OSC) and Fourier-transform infrared (FTIR) spectroscopy are given in the Supporting Information.

2.3. Catalytic performance testing

The evaluation of the catalytic performance of the activated samples (reduced at 400 °C under a 20% H_2/He flow) in the PROX reaction were carried out by using a tubular flow reactor (ID 9 mm) working at atmospheric pressure. For the standards experiments the catalyst (100 mg) sieved to 160–250 μm and diluted with quartz (bed volume of 1.5 cm^3) was pretreated under the reaction mixture at 120 °C for 2 h. The light-off experiments were carried out under a weight hourly space velocity (WHSV) of 60,000 $cm^3\ g^{-1}\ h^{-1}$, by increasing the reaction temperature from 40 to 120 °C. CO conversion and selectivity were recorded after a stabilization period of 40 min at each temperature. Two different feed gas mixtures were used in each investigated reaction as follows: i) 1% CO, 1% O_2 and 50% H_2 in a model PROX reaction and (ii) 1% CO, 1% O_2, 50% H_2, 20% CO_2 and 15% H_2O in a realistic PROX reaction. The stability tests over the most active formulations were performed under the realistic PROX conditions at 80 °C.

Turnover frequency (TOF) and activation energy (E_a) were estimated using reaction mixture conditions corresponding to CO total oxidation (COTOX), 1% CO and 1% O_2 diluted in He, and the model PROX conditions. For these experiments the reduced catalyst was pretreated under the reaction mixture at 200 °C for 4 h. In order to ensure differential reactor conditions only low CO conversion values have been considered (< 15%). Mears analyses were performed to ensure the absence of both mass and heat transfer limitations (Table S1 and Table S2). TOF values were calculated as the activity data per mole of surface gold, as determined by HAADF.

The water vapor was generated by a GILSON 307 pump. The analysis system with a detection limit of 10 ppm consisted of a Gas Chromatograph (Agilent Technologies 490 Micro GC). CO conversion, O_2 conversion and selectivity to CO_2 (X_{CO} and X_{O2} and, S_{CO2}, respectively) values were calculated, where F^{in} and F^{out} represent the inlet and outlet molar flows, respectively, and "λ" is the oxygen excess, according to the

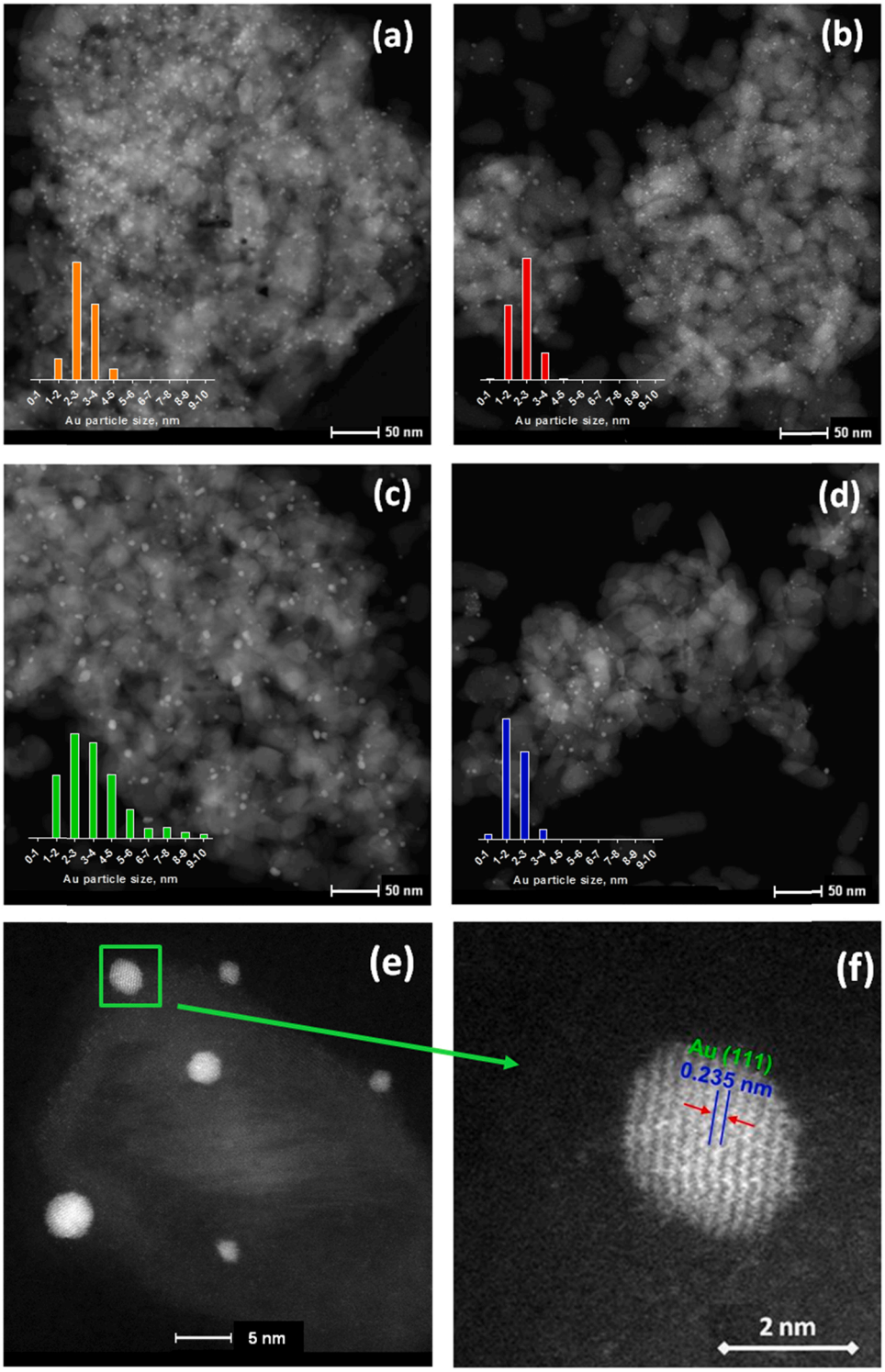

Fig. 1. (a) HAADF images and Au NPs size distributions for (a) Au/HAP, (b) Au/La(0.9)/HAP, (c) Au/La(3.4)/HAP and (d) Au/La(6.6)/HAP catalysts. (e) and (f) correspond to high magnification HAADF images for the Au/La(3.4)/HAP catalyst.

following expressions:

$$X_{CO} = \frac{F_{CO}^{in} - F_{CO}^{out}}{F_{CO}^{in}} \times 100 \quad (1)$$

$$X_{O2} = \frac{F_{O2}^{in} - F_{O2}^{out}}{F_{O2}^{in}} \times 100 \quad (2)$$

$$S_{CO2} = \frac{X_{CO}}{X_{O2}} \times \frac{1}{\lambda} \times 100 \quad (3)$$

$$\lambda = 2 \times \frac{F_{O2}^{in}}{F_{CO}^{in}} \quad (4)$$

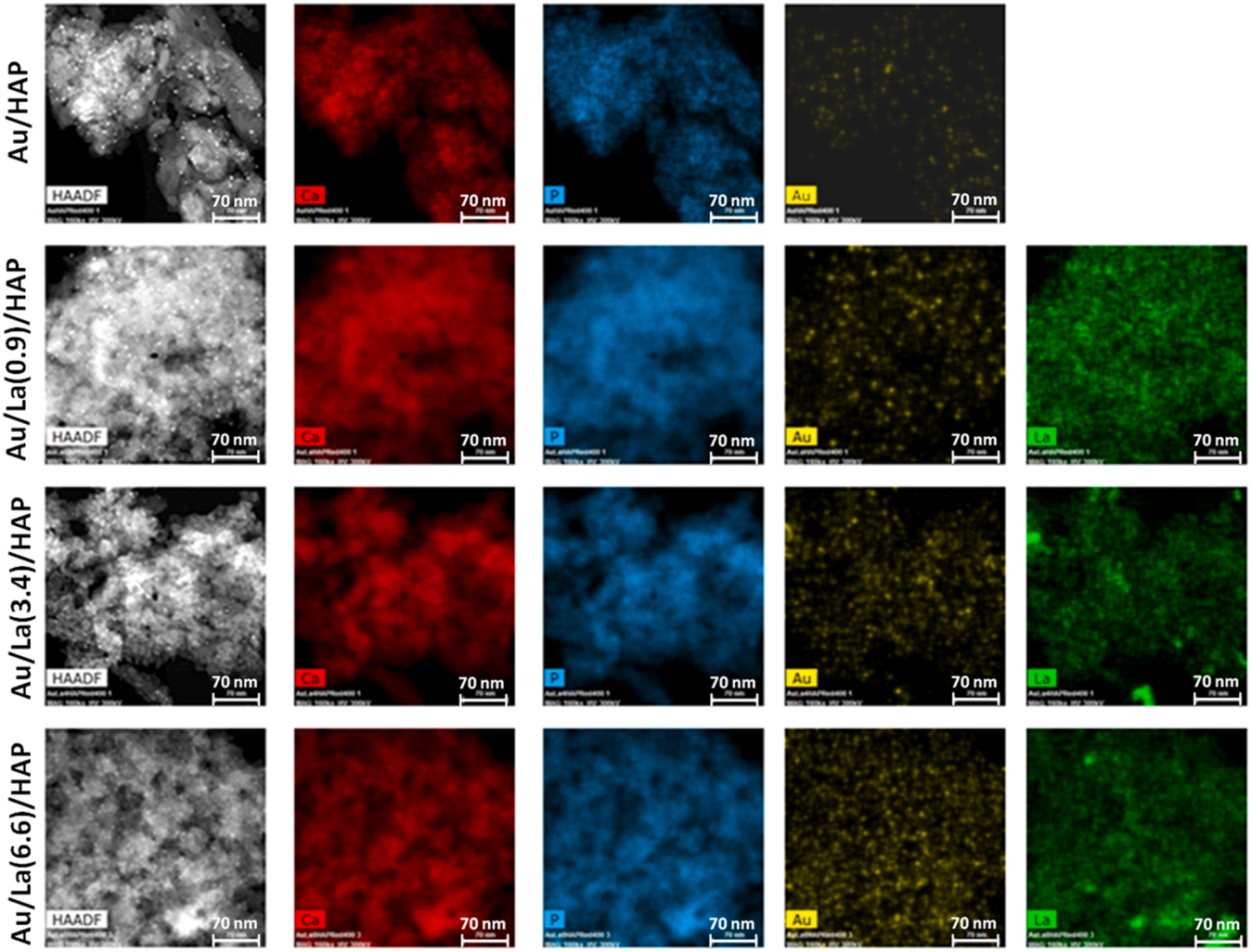

Fig. 2. HAADF images and the corresponding color maps for Ca, P, Au and La, given by X-EDS, for the reduced Au/La(x)/HAP samples.

3. Results and discussion

3.1. Characterization of the activated catalysts

The N_2 physisorption experiments for the reduced Au/La(x)/HAP samples show that their isotherms and hysteresis loops are very similar (Fig. S1). Table 1 lists the textural data obtained from the analysis of these isotherms. Regarding the effect of the lanthanum addition, a significant decrease in the BET surface area, from 56 $m^2\ g^{-1}$, for Au/HAP, to 43 $m^2\ g^{-1}$, for Au/La(6.6)/HAP, is found. In parallel, the mean pore diameter is slightly shifted towards higher values with the progressive addition of lanthanum. The XRD patterns for the synthesized HAP (Fig. S2) are identical to those of the apatite structure (JCPDS 01–082–2956). Regarding the reduced Au/La(x)/HAP samples, besides the HAP peaks, their patterns show a very weak diffraction peak, at 38.5°, ascribed to the most intense reticular plane (111) of metallic Au (JCPDS 00–004–0784). In parallel, no diffraction peak due to lanthanum phases can be observed, which suggests their deposition in highly dispersed forms.

Fig. 1(a-d) displays the HAADF images and the Au particle size distribution for all investigated samples. In all cases, quasi spherical NPs of gold can be observed. However, their distribution seems to depend on the La loading. The smallest Au NPs (1.9 ± 0.5 nm) are observed on the La-rich sample, whereas the Au/La(3.4)/HAP sample exhibits the largest particles (3.6 ± 1.8 nm) (Table 1). Moreover, in good agreement with the XRD results, in typical HAADF-STEM high magnification images for Au/La(3.4)/HAP sample, we can visualize lattice spacing (0.235 nm) corresponding to the (111) plane of deposited Au nano-crystallites (Fig. 1e and f).

To figure out the distribution of La species, the samples have also been analyzed by combining HAADF and X-EDS techniques. Fig. 2 displays HAADF images and their corresponding X-EDS maps showing the distribution of Ca, P, Au and La elements, respectively. As expected, in consistency with the XRD results, the La EDX map for the Au/La(0.9)/HAP sample reveals that lanthanum is homogeneously dispersed. However, at higher La contents (3.6–6.6 wt%), some local concentrations start to take place, indicating a possible tridimensional growth of La_2O_3 crystallites. The absence of the latter from the XRD patterns was probably due to their small relative density.

The XPS surface analyses of the reduced samples, Fig. 3a, show that they mainly comprise metallic gold particles (Au°), since their Au 4 $f_{7/2}$ features are peaked around 83.5 ± 0.2 eV [1,15]. Moreover, data of Table 2 reveal that the Au/La(3.4)/HAP sample exhibits the broadest Au 4f7/2 peak (FWHM = 2.9 eV), indicating a large heterogeneity in Au environments. This heterogeneity would mainly be linked to the presence of a relatively broad size distribution of the Au NPs found on this sample, as assessed by HAADF. The La $3d_{5/2}$ spectra for all La-modified samples exhibit a main photoemission peak near 835.6 ± 0.1 eV (Fig. 3b and Table 2), which suggests the presence of La^{3+} ions from La_2O_3 species [7]. Besides, as deduced from the data of Table 2, the estimated surface La/P atomic ratio systematically increases with the addition of lanthanum, indicating that there is no segregation of the La species [17].

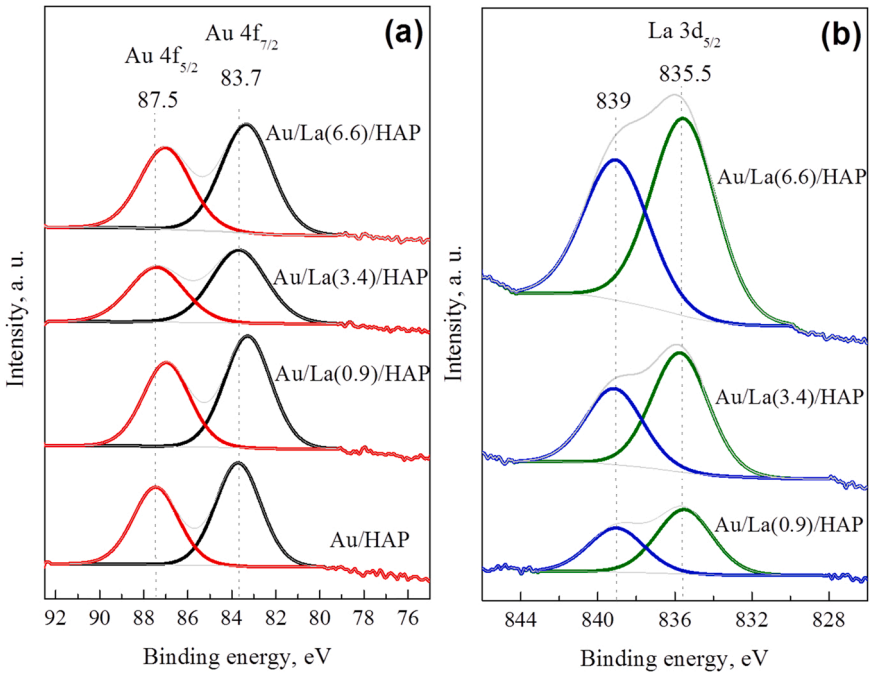

Fig. 3. XPS spectra recorded in (a) Au 4 f and (b) La $3d_{5/2}$ regions for the reduced Au/La(x)/HAP catalysts.

Table 2
XPS data for the reduced Au/La(x)/HAP catalysts.

Catalyst	Au 4 $f_{7/2}$, eV	Au 4 $f_{5/2}$, eV	FWHM Au 4 $f_{7/2}$, eV	La $3d_{5/2}$, eV	FWHM La $3d_{5/2}$, eV	Au/P	La/P	Ca/P
Au/HAP	83.7	87.5	2.4	–	–	0.019	–	1.53
Au/La(0.9)/HAP	83.3	87.0	2.5	835.5	3.41	0.022	0.041	1.50
Au/La(3.4)/HAP	83.7	87.4	2.9	835.7	3.46	0.020	0.092	1.49
Au/La(6.6)/HAP	83.3	87	2.7	835.5	3.96	0.031	0.133	1.47

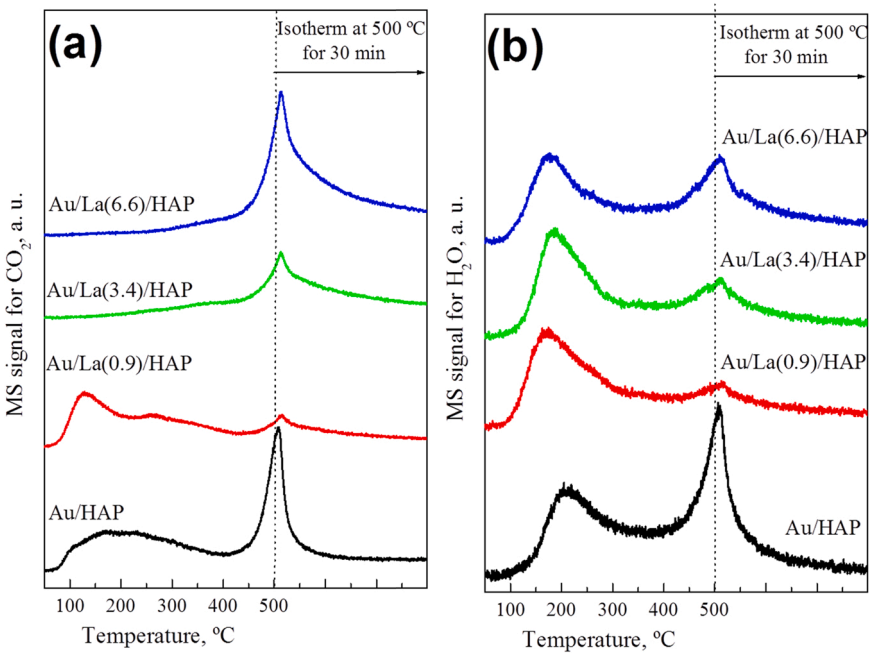

Fig. 4. (a) CO_2 and (b) H_2O desorption profiles, during CO-TPD experiments, for the reduced Au/La(x)/HAP catalysts.

These results would imply that lanthana species form multilayers covering the most of the support surface. However, the tridimensional forms, detected on the La-rich samples by HAADF, do not seem to be dominant phases.

The thermal stability of adsorbed CO on the reduced samples was investigated by CO-TPD techniques. The corresponding profiles

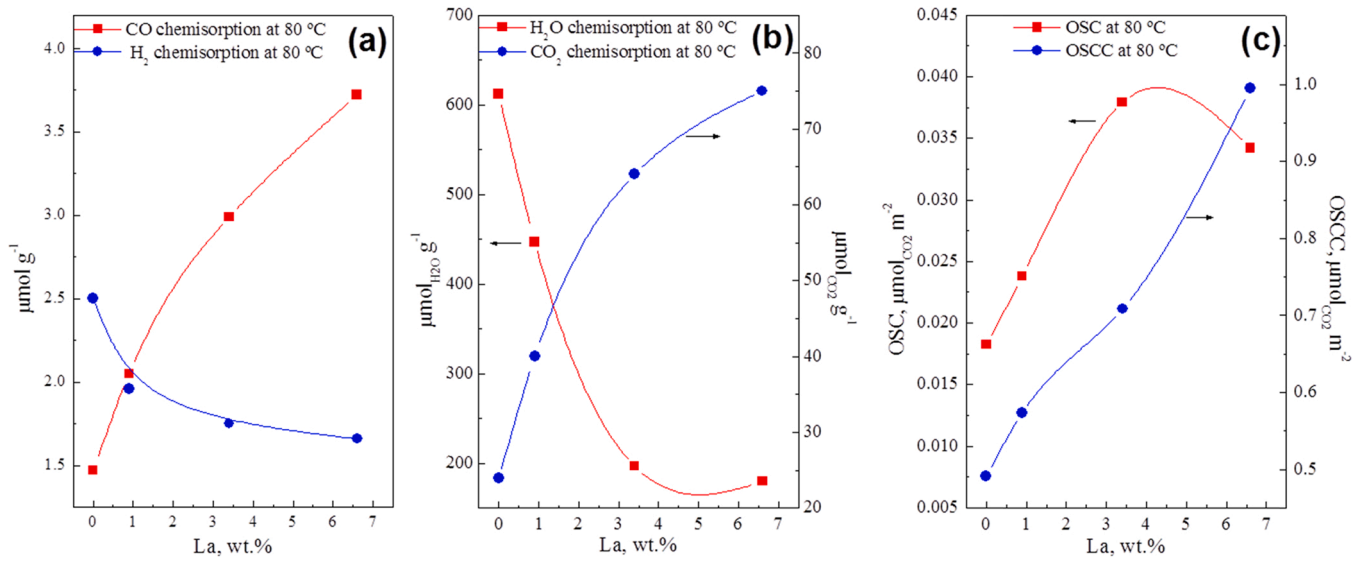

Fig. 5. Evolution of (a) CO_2 and H_2O chemisorption capacity and (b) OSC and OSCC as a function of La content, measured at 80 °C.

presenting the formation and release of CO_2 and water are shown in Fig. 4a and b, respectively. Interestingly, the diagrams for Au/HAP and Au/La(0.9)/HAP samples exhibit large amounts of CO_2 desorbed at low temperatures (< 400 °C). In parallel, significant amounts of H_2O are observed in the desorbing gas (Fig. 4b). In accordance with previous reports [7,18], these results suggest the reaction of adsorbed CO with surface hydroxyl groups, yielding CO_2 and H_2O and leaving hydroxyl vacant sites (Eq. (5)). By contrast, though they also produce large amounts of H_2O, no desorption peaks due to CO_2 can be observed in the case of the La-rich samples, Au/La(3.4)/HAP and Au/La(6.6)/HAP, at low temperatures (< 400 °C). This behavior can be associated with the absence of weak-strength basic sites and the main occurrence of strong basic sites on these two samples, over which thermally stable chemisorbed carbonates species are retained [7]. This observation is very consistent with the results of the FTIR studies to be commented below.

$$CO + 2OH^- \rightarrow CO_2 + H_2O + 2\square^- \quad (5)$$

In order to quantify the extent of the interaction of the gold catalysts with the PROX mixture components volumetric chemisorption studies by using CO, H_2, H_2O and CO_2 probe molecules have been carried out (Figs. 5a,b). The progressive addition of lanthanum leads to a subtle increase in the amounts of chemisorbed CO, whereas it weakens the interaction of the catalysts with H_2 (Fig. 5a). Since the observed trend is not proportional to the dispersion of Au particles, observed by HAADF, the gold particle size effect on the density of H_2 and CO adsorbed molecules can be disregarded [19]. The interaction of the catalysts with the two probe molecules is rather dependent on the nature of specific chemisorption sites, most probably those hosted by the Au-HAP and/or

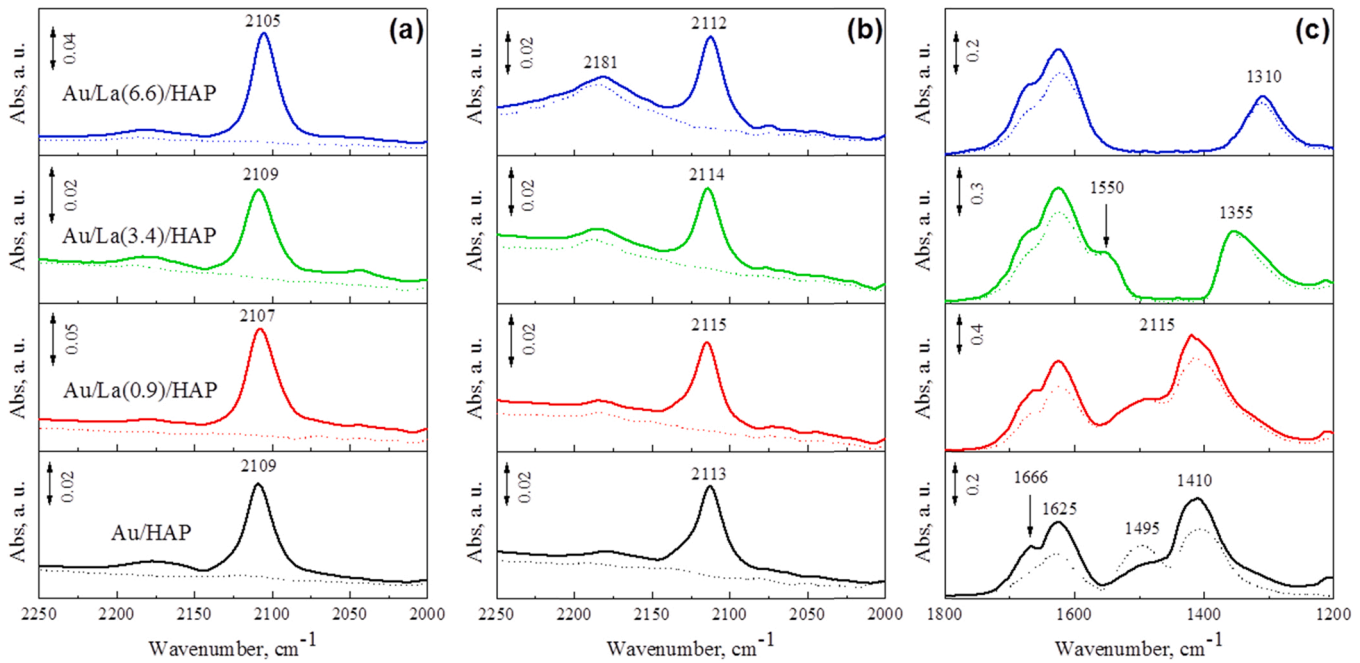

Fig. 6. Carbonyl FTIR spectra for the reduced Au/La(x)/HAP catalysts recorded at 30 °C after 30 min exposure to (a) CO adsorption (750 ppm) and (b) CO + O_2 mixture (750 ppm and 3%, respectively). Dashed lines correspond to the spectra recorded after 30 min under N_2 purge flow. (c) Spectra corresponding to the carbonate region under CO + O_2 mixture.

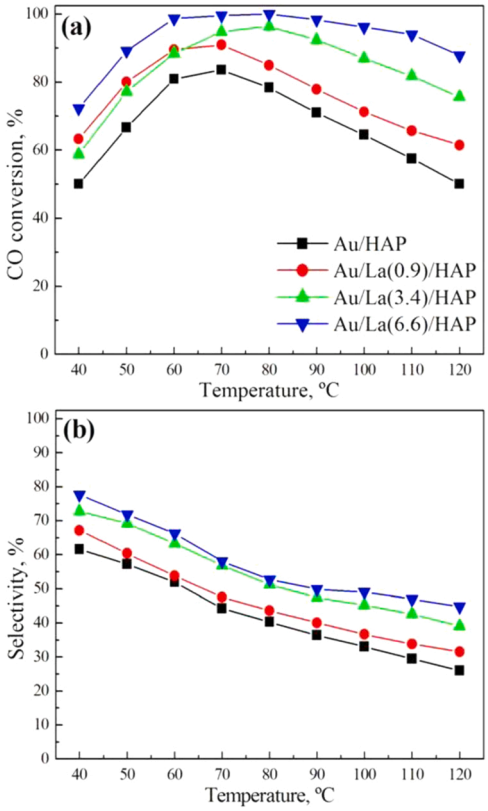

Fig. 7. Catalytic performance of the Au/La(x)/HAP catalysts in ideal PROX conditions: (a) CO conversion and (b) selectivity towards CO_2 production. Reaction mixture: 1% CO, 1% O_2 and 50% H_2, balanced in He (WHSV = 60,000 $cm^3\ g^{-1}\ h^{-1}$).

Au-La_2O_3 interfaces. In line with our proposal, a previous report on an Au/Ce-Tb-Zr system claimed that the CO adsorption capacity of the Au NPs was strongly influenced by the redox properties of the support, being much smaller over the non-reducible ones [20]. Fig. 5b shows the evolution of the adsorption capacity of H_2O and CO_2 with the La content. Interestingly, the adsorption capacity for H_2O decreases with increasing the lanthanum loading. By contrast, the surface density of CO_2 adsorption sites significantly increases with lanthanum, which is consistent with the increase of the number of surface basic sites.

The oxygen storage capacity complete (OSCC) and oxygen storage capacity (OSC) studies performed over the reduced Au/La(x)/HAP catalysts are summarized in Fig. 5c. It should be noted that the OSCC experiments allow the quantification of maximum reducibility of the catalysts while the OSC quantifies the most reactive of surface oxygen atoms. As expected, the unpromoted sample shows the lowest OSCC and OSC values (0.5 and 0.018 $\mu mol_{CO2}\ m^{-2}$). The progressive addition of La markedly improves the maximum reducibly of the catalysts, reaching an OSCC value close to 1 $\mu mol_{CO2}\ m^{-2}$ over the La-rich sample (Au/La (6.6)/HAP). It is clear that the defects generated in the lanthana phase provide additional sites for oxygen storage. This also significantly increases the density of the most labile oxygen sites, giving a maximum on the Au/La(3.4)/HAP sample (OSC of 0.038 $\mu mol_{CO2}\ m^{-2}$). It should be outlined that the OSC superiority of the latter means that, though comprising the largest Au particle sizes, it bears a high density of labile oxygen stored at the Au-La_2O_3 interface, which in turn easily reacts or migrates onto the Au particle surface for CO oxidation [21]. In this sense, it seems that the very reactive nature of the generated interface does compensate the observed low metallic Au dispersion.

To gain further insight into the nature of CO-Au interactions, further CO adsorption experiments were carried out using FTIR spectroscopy (Fig. 6). In good agreement with the XPS data, the CO adsorption over

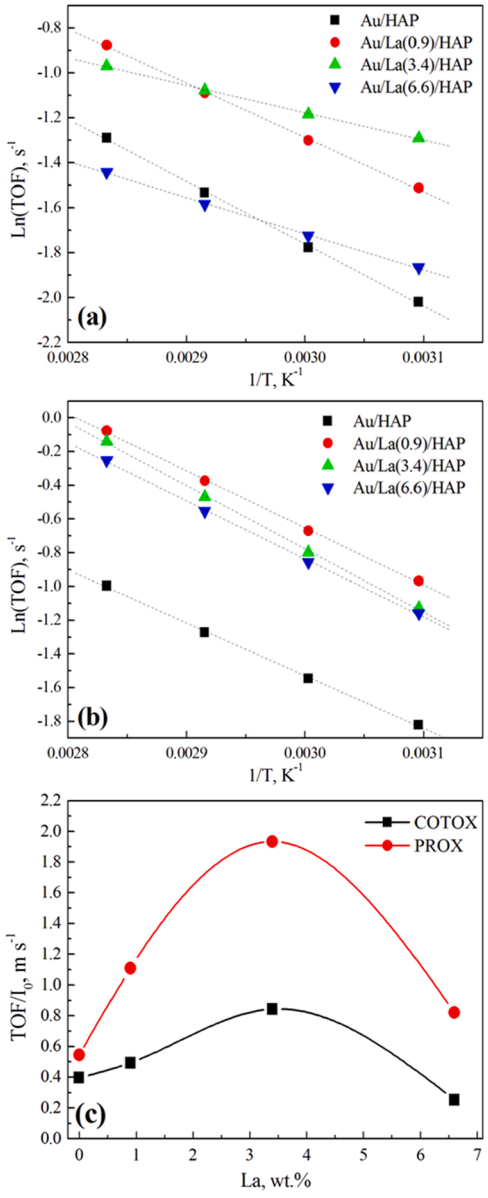

Fig. 8. Arrhenius plots for (a) COTOX and (b) COPROX over the Au/La(x)/HAP catalysts. (c) Dependence of TOF/I_0 ratio on La loading at 80 °C.

the Au/La(x)/HAP catalysts gives rise to a strong FTIR band in the wavenumbers range of 2105–2109 cm^{-1} (Fig. 6a), which can be ascribed to metallic Au species [1]. After purging with N_2 flow for 30 min, it completely disappears from the spectra of all analyzed samples. In the presence of oxygen, however, this main feature slightly shifts towards higher wavenumbers (2112–2115 cm^{-1}) (Fig. 6b). The observed displacement would imply a change in the oxidation state of Au, from metallic to electropositive $Au^{\sigma+}$ species [1,33,34]. Previous reports pointed out that these $Au^{\sigma+}$ sites are actually composed of layered surface Au^+ ions and metallic Au NPs [33,34]. Interestingly, all La-modified samples exhibit an additional CO adsorption band, occurring near 2181 cm^{-1}, which resists N_2 purge, consistent with the presence of more positively charged Au cationic sites [1,22,23,32]. Interestingly, its intensity increases with the progressive addition of La, indicating its close contact with lanthana. Centeno et al. [22] detected a similar feature over an Au/CeO_2/Al_2O_3 catalyst under CO oxidation reaction conditions, peaked around 2180–2184 cm^{-1}, which was assigned to some carbonyls adsorbed on Au^+ cationic sites. Over Au supported on a non-reducible support (Al_2O_3) Venkov et al. [23]

Table 3
COTOX and PROX kinetic data for the Au/La(x)/HAP catalysts.

Catalyst	COTOX[a]		PROX[b]		
	Ea, kJ mol^{-1}	TOF, mol_{CO} $molAu^{-1}$ s^{-1}	Ea, kJ mol^{-1}	TOF[c],mol_{CO} mol_{Au}^{-1} s^{-1}	TOF[d], mol_{H2} mol_{Au}^{-1} s^{-1}
Au/HAP	22.9	0.27	26.0	0.37	0.52
Au/La(0.9)/HAP	20.1	0.41	28.1	0.92	0.70
Au/La(3.4)/HAP	10.1	0.38	31.1	0.87	0.25
Au/La(6.6)/HAP	13.3	0.24	28.6	0.78	0.21

[a] Feed gas: 1% CO and 1% O_2, balanced with He.
[b] Feed gas: 1% CO, 1% O_2 and 50% H_2, balanced with He.
[c] TOF estimated for CO oxidation at 80 °C.
[d] TOF estimated for H_2 oxidation at 80 °C.

reported a FTIR band at somewhat lower wavenumber (2175 cm^{-1}). It seems that over our La-modified samples the metallic Au NPs are partially oxidized under the reaction mixture, generating a fraction of irreversible CO adsorption sites. Mihaylov et al. [33] demonstrated that in an Au/La_2O_3 system the oxidation of gold during the low temperature CO oxidation reaction occurred because CO_2 product did act as an oxidizing agent.

A special attention has also been paid to the evolution of the bands due to carbonates species (1200–1800 cm^{-1}), under CO oxidation conditions (Fig. 6c). All spectra show a set of absorption bands in the range of 1310–1410 cm^{-1} and 1550–1670 cm^{-1}, associated with the accumulation of monodentate and bidentate carbonate, respectively [18,35]. However, the Au/HAP and Au/La(0.9)/HAP samples exhibit an additional feature at 1495 cm^{-1}, ascribed to bicarbonate adsorbed on weak-strength basic sites [35]. The presence of the latter that can only be unequivocally identified on these two samples is in good agreement with the CO-TPD results.

3.2. Catalytic performance

Fig. 7a,b display the profiles of CO conversion and selectivity toward CO_2 formation, respectively, under an ideal PROX mixture. It should be noted that, prior their testing, the Au/La(x)/HAP catalysts were activated under reducing atmosphere (20% H_2/He) at 400 °C for 2 h. Interestingly, the progressive addition of lanthanum systematically improves the activity and selectivity, which evidences its promoting effect. Over the highest La loading (Au/La(6.6)/HAP) the CO conversion reaches 100% and the corresponding window is the widest one, extending from 60 to 80 °C. However, among all tested catalysts, the highest T_{max} value (80 °C) is observed for the Au/La(3.4)/HAP catalyst, which is consistent with the presence of the largest Au particles (3.6 ± 1.8) on this sample.

Apparent activation energy (E_a) for COTOX and PROX reactions, obtained by linear regression of Arrhenius plots, have been estimated under differential reactor conditions (Fig. 8a and b, respectively) and

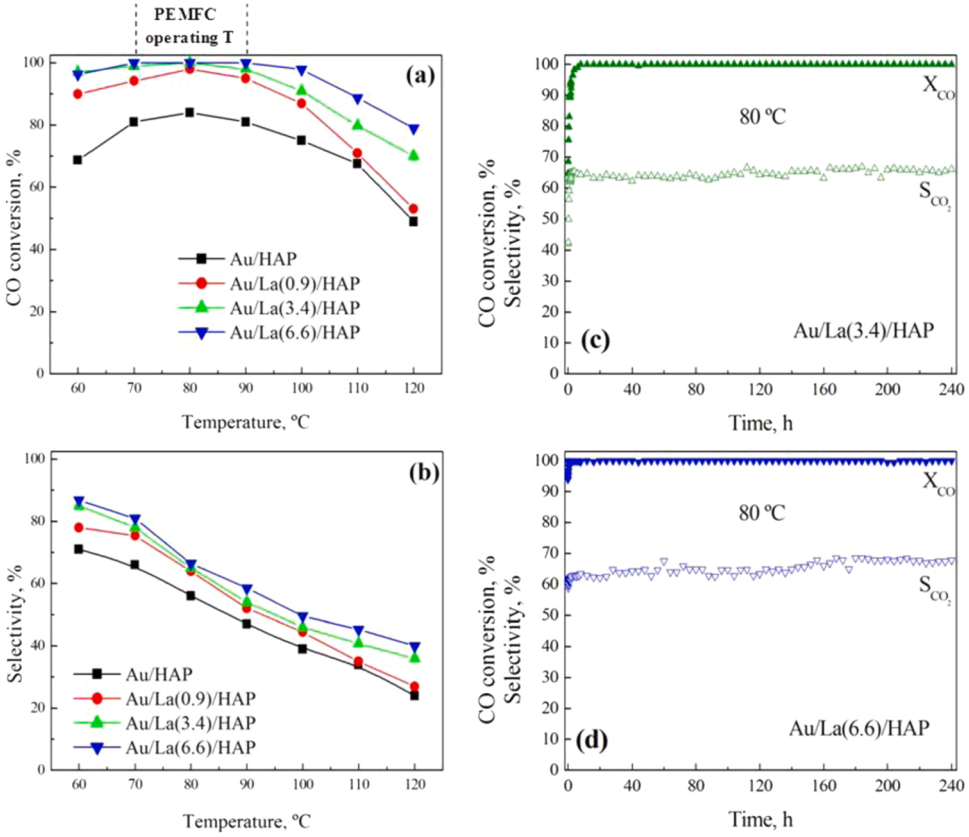

Fig. 9. Catalytic performance of the Au/La(x)/HAP catalysts in realistic PROX conditions: (a) CO conversion and (b) selectivity towards CO_2 production. Reaction mixture conditions: 1% CO, 1% O_2, 50% H_2, 15% H_2O and 20% CO_2, balanced in He (WHSV = 60,000 cm^3 g^{-1} h^{-1}). (c) and (d) correspond to the stability tests performed over Au/La(3.4)/HAP and Au/La(6.6)/HAP, respectively.

Table 4
Comparison of the PROX performance of the Au/La(x)/HAP catalysts with different Au catalyst formulations reported in the literature.

Catalyst	Au, wt%	Feed gas composition, %	WHSV, $cm^3\ g^{-1}\ h^{-1}$	T, °C	X_{CO}, %	S_{CO2}, %	TOS, h	Ref.
		$CO/O_2/H_2/CO_2/H_2O$						
Au/HAP	1.09	1/1/50/20/15	60,000	80	84	57	48	This work
Au/La(0.9)/HAP	1.10	1/1/50/20/15	60,000	80	95	63	160	
Au/La(3.4)/HAP	1.10	1/1/50/20/15	60,000	80	100	66	240	
Au/La(6.6)/HAP	1.10	1/1/50/20/15	60,000	80	100	66	240	
Au/F_1-HAP	1.08	1/1/50/20/15	60,000	80	100	62	70	[1]
Au/Fe_2O_3	5	0.9/0.9/50/22/4.7	12,000	80	99.5	51	14	[4]
Au/Fe_2O_3	3.3	1.03/1.37/70.1/24/3	n. d.	80	100	n. d.	200	[29]
3Au/MnAl	3.1	1/1/40/20/10	40,000	80	95	55	40	[30]
$Au/La\text{-}Al_2O_3$	0.82	1/1/40/20/10	60,000	80	62	n. d.	20	[16]
Au/Fe_2O_3	4.4	1/1/40/20/10	60,000	80	47	n. d.	20	[16]
Au/CeO_2	0.05	1/1/40/20/10	50,000	80	20	n. d.	50	[6]
$1\%Au/CeO_2$	1	1/1/40/2/2.6	30,000	80	92	62	50	[31]

summarized in Table 3. Under the H_2-free CO oxidation conditions (COTOX) the E_a values are found to be ranging between 10.1 and 22.9 kJ mol^{-1}, in agreement with those reported in previous works [24,25]. The relatively lower E_a values observed over the La-rich samples (10.1–13.3 kJ mol^{-1}) would imply differences in the mechanism pathway with respect to that of Au/HAP and Au/La(0.9)/HAP catalysts (22.9 and 20.1 kJ mol^{-1}, respectively). Previous reports claimed that oxygen activation is facilitated at the metal/support interface, which is widely regarded as the key step in the CO oxidation reaction [3,5]. The OSC data support this interpretation, since the La-rich samples exhibit the largest amounts of labile oxygen assumed to be hosted at the metal/support interface (Fig. S3). Besides, in agreement with our FTIR data, Au/HAP and Au/La(0.9)/HAP catalysts bear additional carbonate species adsorbed on weak-strength basic sites. We speculate that their competitive adsorption could hinder the effective participation of some active sites. In addition, the difference between the catalysts may be linked to the nature of the Au species involved in the activation of the reaction intermediates. In this sense, the low activation energy observed over the La-rich catalysts can also be correlated with the presence of large density of Au^+ cationic sites, as assessed by FTIR, which probably facilitate the CO oxidation. In line with our observation, previous reports claimed that cationic gold might be involved in CO oxidation, irrespective of the reaction temperature [27,28,33]. Guzman et al. [27] even pointed out the vital role of the cationic forms of gold, since their reduction by CO as a reactant provoked a diminution in the catalytic activity. In their study on the activity of Au/La_2O_3 catalysts Mihaylov et al. [33] showed that O_2 was not activated on metallic Au, but cationic gold sites somehow did assist its effective activation.

On the other hand, as deduced from the data reported in Table 3, irrespective of the Au catalyst there is a significant increase in the E_a values under PROX compared with COTOX conditions, becoming close to each other (26–31.1 kJ mol^{-1}). The observed difference in the activation energy can be linked to the presence of water (H_2 oxidation product) under PROX conditions. In their study on the effect of water addition on the CO oxidation over a Au/TiO_2 catalyst, Saavedra et al. [3] evidenced the occurrence of a water-mediated reaction mechanism, in accordance with which, the decomposition of *COOH intermediate involves a proton transfer (from *COOH to water) which represented a rate-determining step. In parallel, TOF values become relatively higher in the presence of H_2, consistent with the promotion of Au active site efficiency. This improvement is more pronounced in the case of La-modified samples, since their activity for PROX is more than twice higher than that for COTOX reaction. According to previous reports, this promoting effect can be explained by the formation of water which accelerates CO oxidation [2,3,24–26]. The produced water, even in small amounts, plays a key role in the CO oxidation by enhancing the activation of oxygen as well as the decomposition of carbonate [1–3]. Besides, it is worth outlining the subtle increase of the TOF values for PROX in the La-modified samples (0.78–0.92 s^{-1}) compared with the monometallic sample (0.37 s^{-1}), indicating the presence of more efficient Au active sites on the former. In addition, in contrast to the monometallic sample, the La-promoted ones prove to be more active for CO oxidation than H_2 oxidation (Table 3), consistent with their higher OSC and CO chemisorption capacities as well as their lower H_2 chemisorption capacity. However, there is no clear correlation between the dispersion of gold NPs and the specific activity. We should conclude that the PROX efficiency dependence on the gold NP sizes becomes secondary, at least in the range of 1.9–3.6 nm. Accordingly, we assume that the efficiency of the Au NPs most likely arises from the occurrence of suitable chemical properties induced by the lanthanum addition. Fig. 8c displays the dependence of the activity per gold atoms at the metal-support interface on lanthanum loading. Note that the metal-support perimeter per metal surface area (I_0) was estimated by using the HAADF data corresponding to at least 250 gold NPs. The obtained results suggest that the sample with the intermediate lanthanum loading (3.4 wt%) provides the most efficient species lying on the metal-support interface. It should be noted that, for this sample, XPS data revealed a large heterogeneity in Au environment. Taking into account the critical value corresponding to a theoretical monolayer of supported lanthanum (5.12 $La^{3+}\ nm^{-2}$), we assume that over the Au/La (3.4)/HAP sample (2.9 $La^{3+}\ nm^{-2}$) a large fraction of HAP support surface (at least 44%) remains uncovered. In other words, on the Au/La (3.4)/HAP sample Au NPs would interact simultaneously with HAP and lanthana sites. By contrast, on the rest of the investigated samples the environment of Au species is rather homogeneous, characterized by a relative abundance of the surface sites of hydroxyapatite support (Au/HAP and Au/La(0.9)/HAP) or lanthana (Au/La(6.6)/HAP).

Fig. 9a,b show the performance of the Au/La(x)/HAP under realistic PROX conditions (in the presence of H_2O and CO_2) in terms of CO conversion and selectivity, respectively. With reference to the model PROX conditions, under realistic PROX mixtures the catalysts show a displacement of the activity window towards higher temperatures. Moreover, a significant increase in the selectivity levels can be observed over the whole investigated temperatures (60–120 °C). The performance of the catalysts maintains the general order observed in the case of ideal PROX conditions. Irrespective of the reaction temperature, the unpromoted catalyst (Au/HAP) shows the lowest activity whereas the La-rich sample (Au/La(6.6)/HAP) results the most active one. The latter achieves 100% conversion and its temperature windows are significantly the widest one, extending from 70° to 90°C.

The stability tests over 240 h period, performed at 80 °C, reveal the robust performance of the Au/La(3.4)/HAP and Au/La(6.6)/HAP catalysts (Fig. 9c and d) compared with Au/HAP and Au/La(0.9)/HAP catalysts (Figs. S4 and S5, respectively). Over the former 100% CO conversion and 66% selectivity can be achieved during realistic PEMFC working conditions. Interestingly, as it can be deduced from Figs. S6-a and S7, a further increase of La loading to reach 8.9 wt% provokes a significant decay in the PROX performance. Likewise, the use of bulk

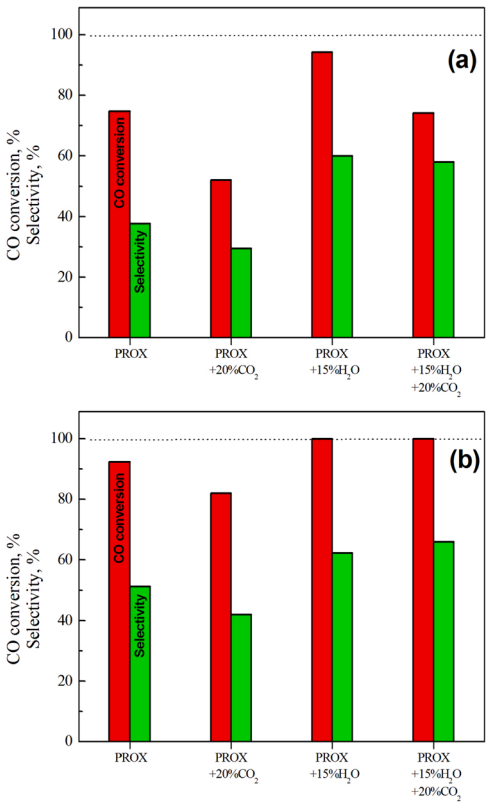

Fig. 10. Effect of H_2O and CO_2 addition on the performance of the (a) Au/HAP and (b) Au/La(3.4)/HAP catalysts in PROX reaction. The standard PROX mixture is composed of 1% CO, 1% O_2 and 50% H_2 balanced in He (WHSV = 60,000 $cm^3\ g^{-1}$).

lanthana as Au catalyst support results in a very poor PROX activity (Fig. 6S-b). In Table 4 our results are compared with those of previous reports from the literature. These data do evidence the superiority of our Au/La/HAP catalyst formulation. In fact, under similar operating conditions, only our previous report dealing with Au/F(x)-HAP pointed out a total elimination of CO, but with somewhat lower selectivity (62%) compared with that achieved in the present study (66%). It can be deduced that improving the surface basicity of the investigated materials through La addition could enhance the selectivity of the investigated catalysts.

Then, we estimate that this simple comparison can open a new window for a potential application of HAP-based catalysts exhibiting a large room of improvement. Moreover, we can highlight that the improvement induced by La addition on the activity of the Au NPs is more evident for our HAP-based catalysts compared with an Au/La-Al_2O_3 system, reported by Lin et al. [16]. This confirms once again the suitability of our synthesized HAP support for realistic PROX conditions. The occurrence of advantageous synergy formed at the interface of Au and the La-modified HAP support represents a key factor to achieve much improved chemical and catalytic properties [39–41].

To figure out the effect of H_2O and CO_2 addition on the performances of the unpromoted and Au/La(3.4)/HAP catalysts, additional experiments were carried out by modifying the composition of the PROX reaction mixture (Fig. 10). Expectedly, the addition of only CO_2 to the PROX mixture provokes a significant decrease of the activity and selectivity of the two samples, which may be attributed to a massive formation of carbonates [1,2,16]. The addition of only water, however, markedly promotes the PROX performance. Importantly, the addition of CO_2 to these water-assisted PROX conditions does not affect the performance of Au/La(3.4)/HAP sample, whereas it leads to a decrease in the conversion values over the unpromoted sample, but no significant changes in the selectivity can be observed. Under these realistic conditions it seems that the effect of water in assisting the CO oxidation active sites only occurs on the La-promoted sample. Previous studies attributed the promotional effect of water on the PROX performance to its capacity to decompose carbonates and in competing with H_2 for adsorption sites [2,3,36]. In our recent study on highly performing Au/F-HAP catalysts we associated their exceptional PROX activity with the improvement of their proton conductivity, which in turn allowed the effective participation of water to assist the reactivity of oxygen [1]. Considering the high ionic conduction of lanthanide oxides [37,38], this interpretation supports the observed high performance of our La-modified samples as well.

4. Conclusions

The viability of gold supported on lanthanum-modified HAP catalysts has been investigated in the PROX reaction. The activation of all samples under reducing atmosphere at 400 °C leads to the deposition of small metallic Au NPs (< 4 nm). The progressive addition of lanthanum induces a subtle increase in the amounts of chemisorbed CO and CO_2, whereas it weakens the interaction of the catalysts with H_2 and H_2O. Moreover, lanthanum seems to improve the reducibility of the catalysts and increases the density of labile oxygen. In contrast to the monometallic sample, FTIR studies show that under CO oxidation conditions Au exists in two distinct forms in the La-promoted samples, namely $Au^{\sigma+}$ and Au^{+} cationic species. The latter form, being located at the Au-La_2O_3 interface, irreversibly adsorbs carbonyl species.

The catalytic tests under both model and realistic PROX conditions show a systematic improvement of the activity and selectivity with lanthanum addition, which evidences its promoting effect. The PROX efficiency dependence on the gold NP sizes is rather secondary, at least in the range of 1.9–3.6 nm, and it seems that the observed improvement most likely arises from the occurrence of suitable chemical properties induced by the lanthanum addition. For instance, the optimal catalysts, namely Au/La(3.4)/HAP and Au/La(6.6)/HAP, achieve 100% CO conversion and 66% selectivity during realistic PEMFC working conditions (80 °C and in the presence of H_2O and CO_2). Moreover, they are exceptionally stable, operating successfully for an extended testing period (240 h).

CRediT authorship contribution statement

Zouhair Boukha: Conceptualization, Investigation, Methodology, Software, Data curation, Writing – original draft preparation, Funding acquisition. **Juan R. González-Velasco:** Conceptualization, Writing – review & editing, Funding acquisition. **Miguel A. Gutiérrez-Ortiz:** Conceptualization, Writing – review & editing, Funding acquisition.

Declaration of Competing Interest

The authors declare that they have no known competing financial interests or personal relationships that could have appeared to influence the work reported in this paper.

Acknowledgements

The financial support from the Basque Government (IT1509-22) is acknowledged. The authors also acknowledge the technical support provided by SGIker (UPV/EHU Advanced Research Facilities/ERDF, EU).

Appendix A. Supporting information

Supplementary data associated with this article can be found in the online version at doi:10.1016/j.apcatb.2022.121384.

References

[1] Z. Boukha, J.R. González-Velasco, M.A. Gutiérrez-Ortiz, Exceptional performance of gold supported on fluoridated hydroxyapatite catalysts in CO-cleanup of H_2-rich stream: High activity and resistance under PEMFC operation conditions, Appl. Catal. B-Environ. 292 (2021), 120142.

[2] J. Saavedra, T. Whittaker, Z. Chen, C.J. Pursell, R.M. Rioux, B.D. Chandler, Controlling activity and selectivity using water in the Au-catalysed preferential oxidation of CO in H_2, Nat. Chem. 8 (2016) 584–589.

[3] J. Saavedra, H.A. Doan, C.J. Pursell, L.C. Grabow, B.D. Chandler, The critical role of water at the gold-titania interface in catalytic CO oxidation, Science 345 (2014) 1599–1602.

[4] P. Landon, J. Ferguson, B.E. Solsona, T. Garcia, S. Al-Sayari, A.F. Carley, A. A. Herzing, C.J. Kiely, M. Makkee, J.A. Moulijn, A. Overweg, S.E. Golunski, G. J. Hutchings, Selective oxidation of CO in the presence of H_2, H_2O and CO_2 utilising Au/α-Fe_2O_3 catalysts for use in fuel cells, J. Mater. Chem. 16 (2006) 199–208.

[5] P. Jing, X. Gong, B. Liu, J. Zhang, Recent advances in synergistic effect promoted catalysts for preferential oxidation of carbon monoxide, Catal. Sci. Technol. 10 (2020) 919–934.

[6] B. Qiao, J. Liu, Y.G. Wang, Q. Lin, X. Liu, A. Wang, J. Li, T. Zhang, J. Liu, Highly efficient catalysis of preferential oxidation of CO in H2-rich stream by gold single-atom catalysts, ACS Catal. 5 (2015) 6249–6254.

[7] Z. Boukha, J.R. González-Velasco, M.A. Gutiérrez-Ortiz, Platinum supported on lanthana-modified hydroxyapatite samples for realistic WGS conditions: on the nature of the active species, kinetic aspects and the resistance to shut-down/start-up cycles, Appl. Catal. B-Environ. 270 (2020), 118851.

[8] Z. Boukha, A. Choya, M. Cortés-Reyes, B. de Rivas, L.J. Alemany, J.R. González-Velasco, J.I. Gutiérrez-Ortiz, R. López-Fonseca, Influence of the calcination temperature on the activity of hydroxyapatite-supported palladium catalyst in the methane oxidation reaction, Appl. Catal. B-Environ. 277 (2020), 119280.

[9] Z. Boukha, J. González-Prior, B. de Rivas, J.R. González-Velasco, R. López-Fonseca, J.I. Gutiérrez-Ortiz, Pd supported catalyst for gas-phase 1,2-dichloroethane abatement: efficiency and high selectivity towards oxygenated products, J. Ind. Eng. Chem. 57 (2018) 77–88.

[10] Z. Boukha, M.P. Yeste, M.Á. Cauqui, J.R. González-Velasco, Influence of Ca/P ratio on the catalytic performance of Ni/hydroxyapatite samples in dry reforming of methane, Appl. Catal. A Gen. 580 (2019) 34–45.

[11] Z. Boukha, J.L. Ayastuy, M. Cortés-Reyes, L.J. Alemany, J.R. González-Velasco, M. A. Gutiérrez-Ortiz, Catalytic performance of Cu/hydroxyapatite catalysts in CO preferential oxidation in H_2-rich stream, Int. J. Hydrog. Energy 44 (2019) 12649–12660.

[12] Z. Boukha, J.L. Ayastuy, M. Cortés-Reyes, L.J. Alemany, M.A. Gutiérrez-Ortiz, J. R. González-Velasco, Catalytic properties of cobalt-promoted Pd/HAP catalyst for CO-cleanup of H2-rich stream, Int. J. Hydrog. Energy 43 (2018) 16949–16958.

[13] Z. Boukha, J.L. Ayastuy, J.R. González-Velasco, M.A. Gutiérrez-Ortiz, Water-gas shift reaction over a novel Cu-ZnO/HAP formulation: Enhanced catalytic performance in mobile fuel cell applications, Appl. Catal. A Gen. 566 (2018) 1–14.

[14] P. Lakshmanan, J.E. Park, B. Kim, E.D. Park, Preferential oxidation of CO in a hydrogen-rich stream over Au/MO_x/Al_2O_3 (M = La, Ce, and Mg) catalysts, Catal. Today 265 (2016) 19–26.

[15] P. Lakshmanan, E.D. Park, Preferential CO oxidation in H_2 over Au/La_2O_3/Al_2O_3 catalysts: the effect of the catalyst reduction method, Catalysts 8 (5) (2018) 183.

[16] Q. Lin, B. Qiao, Y. Huang, L. Li, J. Lin, X.Y. Liu, A. Wang, W.-C. Li, T. Zhang, La-doped Al_2O_3 supported Au nanoparticles: highly active and selective catalysts for PROX under PEMFC operation conditions, Chem. Commun. 50 (2014) 2721–2724.

[17] Z. Boukha, L. Fitian, M. López-Haro, M. Mora, J.R. Ruiz, C. Jiménez-Sanchidrián, G. Blanco, J.J. Calvino, G.A. Cifredo, S. Trasobares, S. Bernal, Influence of the calcination temperature on the nano-structural properties, surface basicity, and catalytic behavior of alumina-supported lanthana samples, J. Catal. 272 (2010) 121–130.

[18] M. Li, Z. Wu, S.H. Overbury, CO oxidation on phosphate-supported Au catalysts: effect of support reducibility on surface reactions, J. Catal. 278 (2011) 133–142.

[19] A. Villa, N. Dimitratos, C.E. Chan-Thaw, C. Hammond, G.M. Veith, D. Wang, M. Manzoli, L. Prati, G.J. Hutchings, Characterisation of gold catalysts, Chem. Soc. Rev. 45 (2016) 4953–4994.

[20] E. del Río, M. López-Haro, J.M. Cíes, J.J. Delgado, J.J. Calvino, S. Trasobares, G. Blanco, M.A. Cauqui, S. Bernal, Dramatic effect of redox pre-treatments on the CO oxidation activity of Au/Ce0.50Tb0.12Zr0.38O2-x catalysts prepared by deposition-precipitation with urea: a nano-analytical and nano-structural study, Chem. Commu. 49 (2013) 6722–9724.

[21] T. Schalow, M. Laurin, B. Brandt, S. Schauermann, S. Guimond, H. Kuhlenbeck, D. E. Starr, S.K. Shaikhutdinov, J. Libuda, H. Freund, Oxygen storage at the metal/oxide interface of catalyst nanoparticles, Angew. Chem. Int. Ed 44 (2005) 7601–7605.

[22] M.A. Centeno, K. Hadjiivanov, H. Tz. Venkov, J.A. Klimev, Odriozola, Comparative study of Au/Al_2O_3 and Au/CeO_2-Al_2O_3 catalysts, J. Mol. Catal. A Chem. 252 (2006) 142–149.

[23] T. Venkov, H. Klimev, M.A. Centeno, J.A. Odriozola, K. Hadjiivanov, State of gold on an Au/Al_2O_3 catalyst subjected to different pre-treatments: an FTIR study, Catal. Commun. 7 (2006) 308–313.

[24] M. Daté, M. Okumura, S. Tsubota, M. Haruta, Vital role of moisture in the catalytic activity of supported gold nanoparticles, Angew. Chem. Int. Ed. 43 (2004) 2129–2132.

[25] E. Quinet, L. Piccolo, F. Morfin, P. Avenier, F. Diehl, V. Caps, J. Rousset, On the mechanism of hydrogen-promoted gold-catalyzed CO oxidation, J. Catal. 268 (2009) 384–389.

[26] J. Lin, B. Qiao, J. Liu, Y. Huang, A. Wang, L. Li, W. Zhang, L.F. Allard, X. Wang, T. Zhang, Design of a highly active Ir/$Fe(OH)_x$ catalyst: versatile application of Pt-group metals for the preferential oxidation of carbon monoxide, Angew. Chem. Int. Ed. 51 (2012) 2920–2924.

[27] J. Guzman, B.C. Gates, Catalysis by supported gold: correlation between catalytic activity for CO oxidation and oxidation states of gold, J. Am. Chem. Soc. 126 (2004) 2672–2673.

[28] J.C. Fierro-Gonzalez, J. Guzman, B.C. Gates, Role of cationic gold in supported CO oxidation catalysts, Top. Catal. 44 (2007) 103–114.

[29] T. Shodiya, O. Schmidt, W. Peng, N. Hotz, Novel nano- scale Au/α-Fe_2O_3 catalyst for the preferential oxidation of CO in biofuel reformate gas, J. Catal. 300 (2013) 63–69.

[30] Y.- Miao, W.- Li, Q. Sun, L. Shi, L. He, J. Wang, G.- Deng, A.- Lu, Nanogold supported on manganese oxide doped alumina microspheres as a highly active and selective catalyst for CO oxidation in a H_2-rich stream, Chem. Commun. 51 (2015) 17728–17731.

[31] A. Luengnaruemitchai, S. Osuwan, E. Gulari, Selective catalytic oxidation of CO in the presence of H_2 over gold catalyst, Int. J. Hydrog. Energy 29 (2004) 429–435.

[32] F. Boccuzzi, A. Chiorino, M. Manzoli, P. Lu, T. Akita, S. Ichikawa, M. Haruta, Au/TiO_2 nanosized samples: a catalytic, TEM, and FTIR study of the effect of calcination temperature on the CO oxidation, J. Catal. 202 (2001) 256–267.

[33] M. Mihaylov, E. Ivanova, Y. Hao, K. Hadjiivanov, B.C. Gates, H. Knozinger, Oxidation by CO_2 of Au° species on La_2O_3-supported gold clusters, Chem. Commun. 2 (2008) 175–177.

[34] M. Mihaylov, B.C. Gates, J.C. Fierro-Gonzalez, K. Hadjiivanov, H. Knozinger, J. Phys. Chem. C 111 (2007) 2548–2556.

[35] J.I. Di Cosimo, V.K. Díez, M. Xu, E. Iglesia, C.R. Apesteguía, Structure and surface and catalytic properties of Mg-Al basic oxides, J. Catal. 178 (1998) 499–510.

[36] B. Schumacher, Y. Denkwitz, V. Plzak, M. Kinne, R.J. Behm, Kinetics, mechanism, and the influence of H2 on the CO oxidation reaction on a Au/TiO2 catalyst, J. Catal. 224 (2004) 449–462.

[37] N. García-Moncada, M. González-Castaño, S. Ivanova, M.Á. Centeno, F. Romero-Sarria, J.A. Ordiozola, New concepts for old reaction: novel WGS catalyst design, Appl. Catal. B Environ. 238 (2018) 1–5.

[38] G. Adachi, N. Imanaka, S. Tamura, Ionic conducting lanthanide oxides, Chem. Rev. 102 (2002) 2405–2429.

[39] J. Luo, Y. Dong, C. Petit, C. Liang, Development of gold catalysts supported by unreducible materials: design and promotions, Chinese, J. Catal. 42 (2021) 670–693.

[40] Y. Wang, B.B. Chen, M. Crocker, Y.J. Zhang, X.B. Zhu, C. Shi, Understanding on the origins of hydroxyapatite stabilized gold nanoparticles as high-efficiency catalysts for formaldehyde and benzene oxidation, Catal. Commun. 59 (2015) 195–200.

[41] H. Tang, J. Wei, F. Liu, B. Qiao, X. Pan, L. Li, J. Liu, J. Wang, T. Zhang, Strong metal-support interactions between gold nanoparticles and nonoxides, J. Am. Chem. Soc. 138 (2016) 56–59.